Gamma Titanium Aluminides 2008
TMS (The Minerals, Metals & Materials Society), 2008

DURABILITY ASSESSMENT OF TiAl ALLOYS

S. L. Draper and B. A. Lerch

NASA - Glenn Research Center, Cleveland, OH 44135 USA

Keywords: Embrittlement, Ballistic Impact, Fatigue

Abstract

The durability of TiAl is a prime concern for the implementation of TiAl into aerospace engines. Two durability issues, the effect of high temperature exposure on mechanical properties and impact resistance, have been investigated and the results are summarized in this paper. Exposure to elevated temperatures has been shown to be detrimental to the room temperature ductility of gamma alloys with the most likely mechanisms being the ingress of interstitials from the surface. Fluorine ion implantation has been shown to improve the oxidation resistance of gamma alloys, and ideally it could also improve the environmental embrittlement of high Nb content TiAl alloys. The effect of F ion implantation on the surface oxidation and embrittlement of a third generation, high Nb content TiAl alloy (Ti-45Al-5Nb-B-C) were investigated. Additionally, the ballistic impact resistance of a variety of gamma alloys, including Ti-48Al-2Cr-2Nb, Ti-47Al-2Cr-2Nb, ABB-2, ABB-23, NCG359E, 95A and Ti-45Al-5Nb-B-C was accessed. Differences in the ballistic impact properties of the various alloys will be discussed, particularly with respect to their manufacturing process, microstructure, and tensile properties.

Introduction

A key milestone [1] in the use of γ-TiAl in aerospace applications was the development and successful engine testing of the "first generation" alloy Ti-48Al-2Cr-2Nb. This alloy has only modest strength but exhibits relatively high ductility, combined with good environmental resistance and manufacturability that make it particularly suitable for low pressure turbine (LPT) blade applications. Since this work, a significant world-wide effort to improve the strength and temperature capability of γ alloys has ensued, and a number of "3rd generation" alloys have been developed. In particular, Gamma Met PX (GMPX), a high Nb-content alloy produced by PLANSEE AG, Austria and based on the TNB alloys developed by GKSS Research Center, Germany [2], has been under evaluation for several NASA programs. During this evaluation, it became clear that an important factor that could limit durability was susceptibility to environmentally induced embrittlement. For example, the room temperature tensile ductility of GMPX was substantially decreased after a simulated service exposure at 800^{o}C for 200 h in air [3].

The purpose of the current work was to assess the durability of GMPX and how it is limited by two important factors. First, the environmental resistance issue will be reviewed and further explored by examining the feasibility of mitigating the embrittlement through halogen ion implantation. Second, the ballistic impact resistance of GMPX was investigated by measuring the extent of cracking as a function of projectile kinetic energy, and also the fatigue life debit due to impact damage. For both environmental embrittlement and impact resistance, the behavior of GMPX will be compared to 1st and 2nd generation alloys.

Materials and Procedures

Environmental embrittlement was simulated on extruded Ti-45Al-5Nb-B-C (at. %) by exposing tensile samples in air at 700 and 800 ºC for 200 h. Additional tests included exposing unprotected samples to 800 ºC for 200 h in dry, ultra-high purity O_2, and exposing samples wrapped in Ta foil to Ar with a purity of 99.999%. Tensile specimens were tested at 23 and 650 ºC using a constant strain rate of 1×10^{-4} s^{-1}. F ion implantation was performed with a beamline technique using 25 keV of energy and a F dose of 2×10^{17} F/cm^2 at the Karl-Winnacker-Insitut der DECHEMA, Frankfurt, Germany [4]. Temperatures were held to less than 200 ºC during implantation to avoid embrittlement.

The impact study involved a variety of alloys made by various processes, resulting in a range of microstructures, Table I. All error bands represent 95% confidence intervals. The first impact project was performed on Ti-48Al-2Cr-2Nb (at.%) (Ti-48-2-2) samples which were cast-to-size in a dog-bone configuration [5]. The flat specimens had a double-reduced gage section with the edges simulating the leading edges of actual LPT airfoils. The samples were processed in a sequence typical for an LPT blade which included an exposure to 650 ºC for 20 h to simulate typical embrittlement at service conditions prior to impact testing. One other alloy, ABB-2, was also manufactured by casting dog-boned shaped samples. To reduce cost and enable testing of other alloys, a machined sample was designed with a similar leading edge configuration. All subsequent samples were machined from cast or forged plates or extruded rods. Specimens were impacted in a ballistic impact rig consisting of a precision gun barrel mounted on a load frame with an attached furnace. Samples were impacted near the specimen edge with either 1.6 or 3.2-mm diameter ball bearings. The ball bearings were annealed for 1 h at 700 ºC to reduce their hardness to ≤ 20 HRC on the Rockwell C scale, which is more representative of possible debris in an engine. The nominal distance from the leading edge to the impact center (X) was 0.51 mm for the small projectile and 0.64 mm for the large projectile but specimen variability and an imprecise fit between the projectile and gun barrel resulted in some deviation in the aimed distance. The specimens were impacted at 260 ºC in air under a tensile load of 70 MPa. After impact, crack lengths were measured on both the front and back sides. As-received and impacted samples were tested in high-cycle fatigue with a frequency of 100 Hz and a load ratio, R, of 0.05 ($R=\sigma_{min}/\sigma_{max}$). Since the fatigue crack growth rate was reported to be the highest for Ti-48Al-2Nb-2Cr at 650 ºC [6], this temperature was chosen for testing to simulate the worst-case scenario. Due to the flat nature of the stress vs. cycles to failure curve for γ-TiAl, step fatigue tests were used to determine the maximum fatigue strength [5, 7-10]. If the sample survived 10^6 cycles, the stress was increased by 14 MPa and run to failure or an additional 10^6 cycles. Fatigue strength was taken as the stress at the next-to-last step, i.e., the stress representing the fatigue threshold.

Results and Discussion

Environmental Embrittlement

The as-extruded GMPX bars had a duplex microstructure with a high volume fraction of lamellar grains, which varied slightly from batch to batch. The lamellar grain size was approximately 20 μm and small (~ 4 μm) γ grains were located in between lamellar colonies for all batches. The room temperature (RT) plastic elongation to failure was significantly affected by the high temperature exposure of GMPX, Table II [3]. At room temperature, the plastic elongation of as-extruded specimens from three batches of material, 16 samples, averaged 1.54 ± 0.29%. The RT plastic elongation decreased to 0.37 and 0.10% after exposure at 700 and 800 ºC

for 200 h, respectively. While the ultimate tensile strength (UTS) of GMPX at RT decreased with high temperature exposure, the reduction in strength was relatively small and was a result of the lower ductility limiting the amount of strain hardening prior to fracture. The fracture morphology was similar for both exposed and unexposed samples with no evidence of intergranular fracture near the sample surface. Examination of longitudinally polished samples revealed a variety of fracture paths including translamellar, interlamellar, and intergranular.

Table I. TiAl Alloy Microstructures

	Processing	**Lamellar Vol. Fraction**	**γ Grain Size, μm**	**Lamellar Colony Size, μm**
Ti-48Al-2Cr-2Nb	Cast-to-Size	0.39 ± 0.06	64.0 ± 2.3	
Ti-47Al-2Cr-2Nb	Machined from cast plate	0.65 ± 0.04	60.3 ± 3.3	
ABB-2 Ti-46.5Al-2.3W-0.5Si	Cast-to-Size	Fully lamellar at edge, duplex in center	Irregular	Large, columnar colonies near edge
ABB-23 Ti-46Al-2W-0.5Si-0.65B	Machined from cast plate	~1		58.5 ± 3.2
NCG359E Ti-46.8Al-1.6Cr-0.7Nb-1.7Ta	Machined from cast plate	0.68 ± 0.11	69.4 ± 7.1	
95A Ti-47Al-2Cr-2Nb-0.2W-0.1B	Machined from forged pancake	~ 1		288 ± 21.4
GMPX Ti-45Al-5Nb-0.2C-0.2B	Machined from extruded rod	0.5 – 1.0	~4	~20

Table II. Tensile Properties

Alloy	**Temp. (°C)**	**σ_y (MPa)**	**σ_{UTS} (MPa)**	**ε_p (%)**
Ti-48Al-2Cr-2Nb – Cast-to-Size	23	326	422	1.70
	650	284	474	5.10
Ti-47Al-2Cr-2Nb - Machined	23	458	536	1.42
	650	355	539	3.4
ABB-2 – Cast-to-Size	23	504	599	0.89
	650	413	571	1.97
ABB-23 - Machined	23	528	589	0.58
	650	440	532	1.07
NCG359E - Machined	23	422	482	1.01
	650	359	524	3.65
95A (K5 based alloy) - Machined	23	417	547	1.12
	650	331	587	3.93
GMPX - Machined	23	947	1070	1.54
	650	775	1015	1.39
GMPX – Exposed to 800ºC for 200h - Machined	23	---	875	0.10
	650	810	964	0.89

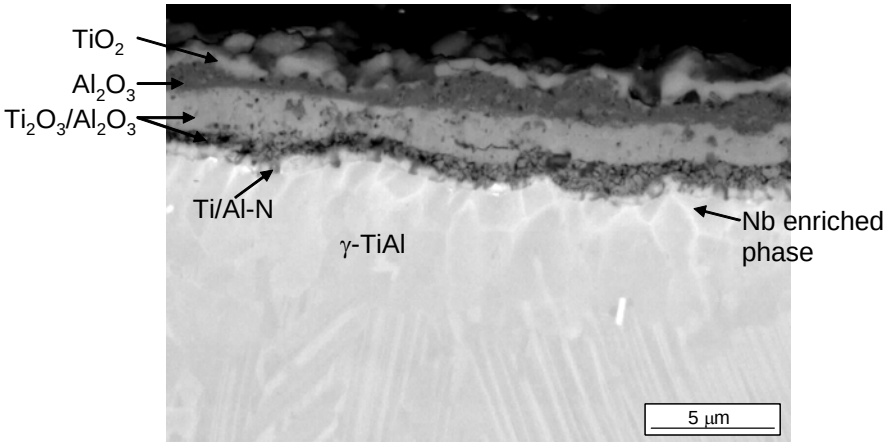

Figure 1. Near surface microstructure of an as-extruded GMPX sample exposed to 800 ºC for 200 h in air**.**

Microprobe analysis revealed oxide and nitride surface layers typical for TiAl alloys [3]. A mixture of TiO_2 and Al_2O_3, 4-5 μm in total thickness, was present after exposure at 800 ºC for 200 h in air, Figure 1. At the oxide-alloy interface, a layer of Ti/Al-N, less than 0.5 μm in thickness, with significant levels of C was observed. Oxygen detectability limit is 0.1 weight percent using wavelength dispersive spectroscopy and within this limit O was only detected in the oxide layer. The near-surface microstructure was nearly 100 % γ-TiAl, enriched in Al and Nb and depleted of Ti. This region extended about 8 - 10 μm beyond the oxide – surface interface. A very fine Nb-enriched phase was also present at the grain boundaries. Beyond a depth of 8 – 10 μm, the microstructure and chemical composition were unchanged from the as-extruded microstructure.

Various mechanisms were investigated [3] as possible sources of embrittlement including: 1) bulk microstructural changes, 2) hydrogen embrittlement, and 3) near-surface effects. The possibility of bulk microstructural changes, such as carbide coarsening, was eliminated by SEM analysis and tensile testing samples machined after exposure. Exposed samples were tested under 99.995% pure Ar and no difference in tensile ductility was found between testing in Ar compared to testing in air. The amount of water vapor in the Ar atmosphere was substantially less than in air and therefore some improvement in ductility should have been observed if water-induced environmental or H embrittlement was a factor. Additional samples were exposed to dry, ultra-high purity oxygen at 800 ºC for 200 h and these samples failed to reach 0.2% offset yield and plastic elongations were minimal, less than 0.05%. Samples exposed to ultra-high purity oxygen revealed internal oxidation and α_2 formation in the near surface region. The oxide scale thickness was not as uniform and varied from less than 1 μm to 15 μm. Hydrogen would not have been present during these exposures, thus eliminating moisture-induced environmental embrittlement as a mechanism. Additional GMPX samples were polished to remove 25, 50, and 75 μm from the surface after exposure to 800 C for 200 h in air. After removal of between 25 – 50 μm from the surface, the ductility was restored. It is clear that the embrittlement is a near surface effect involving oxygen. Microstructural variations were only observed within ~10 μm of the oxide/metal interface but removal of more than 25 μm was required to completely restore the ductility.

The loss of room temperature ductility following high temperature exposure has been reported for other TiAl alloys previously [11-13]. Kelly et al. [12] observed the ductility of Ti-48-2-2 drops in half after exposure to 649 ºC for 16h. The embrittlement issue has not apparently been of great concern as the low ductility has only been observed at test temperatures

below 200 ºC, a regime of little concern in service. However, GMPX has a more substantial room temperature ductility reduction than previous alloys, and also exhibits reductions in fracture toughness and ductility at testing temperatures as high as 650 ºC [3].

Coatings to improve oxidation resistance of TiAl are often brittle in nature and have the potential to degrade mechanical properties. Halogen ion implantation has been shown to improve the oxidation resistance of γ - TiAl without affecting the creep properties [4]. The halogen promotes the formation of gaseous aluminum halides and then the aluminum halides diffuse outward through cracks and pores of the normal oxide scale, oxidizing to Al_2O_3. Both Cl and F have been shown to promote a transition to a protective alumina after an initial TiO_2 + Al_2O_3 scale. Since F provides enhanced protection under thermocyclic oxidation and wet environments, it was chosen to study the effect of the ion implantation on the RT embrittlement of GMPX after high temperature exposure. Two samples were tested in the as-implanted condition and two after an exposure of 800ºC for 200 h, Figure 2. While the room temperature ductility of the F ion implanted sample was similar to as-received with 2.2% plastic elongation, the samples exposed to 800 ºC for 200 h failed to reach a yield stress and had 0% plastic elongation. The F ion implanted plus exposed samples showed degradation even worse than as-received plus exposed samples. The surface of the ion implanted sample is shown in Figure 3. The surface oxide consisted only of Al_2O_3, not the typical mixed scale of Al_2O_3 + TiO_2 (Figure 1) observed on TiAl alloys. Similar to the samples exposed to ultra-high purity oxygen, α_2 was present at the TiAl/oxide interface whereas an α_2 depleted region is typical for GMPX after high temperature exposures [3]. Al was depleted in the near surface region of the F ion implanted sample, consistent with the halogen effect in which the halogen pulls Al from the TiAl to form a gaseous aluminum halide, $AlF_{(g)}$. In summary, while the F ion implantation treatment did not affect the tensile properties of GMPX, the treatment did not protect the alloy from high temperature exposure.

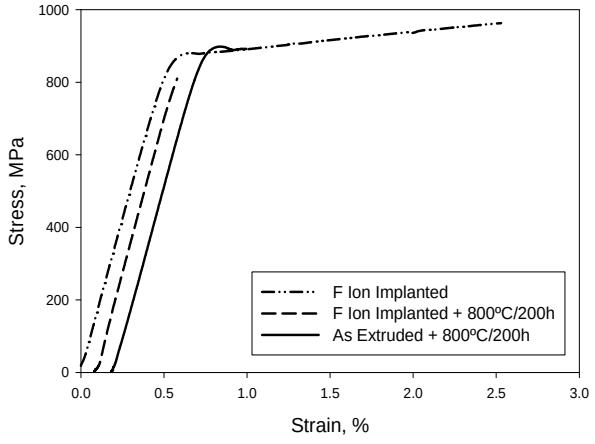

Figure 2. Tensile properties of F ion implantated samples before and after exposure at 800 ºC for 200 h. Starting strain offset.

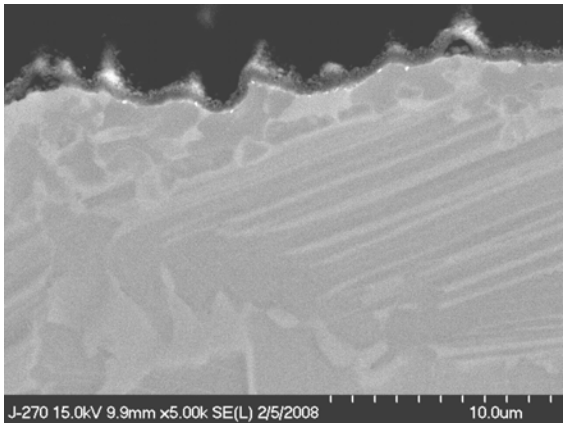

Figure 3. SE image of surface of F ion implanted GMPX exposed to 800 ºC for 200 h.

Ballistic Impact Resistance

Another aspect of TiAl durability, ballistic impact resistance, has been a research area for more than a decade at NASA - Glenn Research Center. The ability of TiAl to withstand ballistic impacts and the effect of the impact damage on fatigue properties has been investigated for a number of γ-TiAl alloys. With the variety of TiAl alloys studied, a comparison between

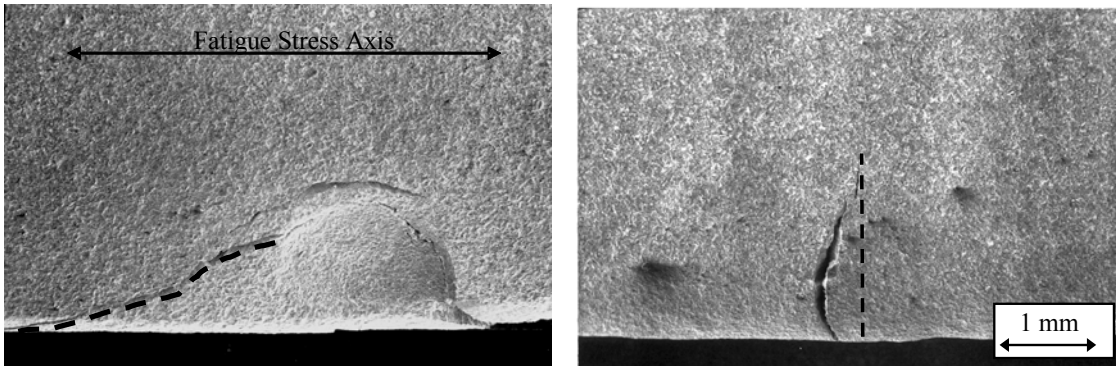

Figure 4. Crack length for (a) Hertzian and corresponding (b) backside crack on cast-to-size Ti-48Al-2-2.

processing, tensile properties, microstructures, and chemistry and their effects on impact and fatigue resistance can be made. A summary of the microstructures and the nominal chemistry for each alloy is given in Table I. The Ti-48-2-2, NCG359E, and GMPX had duplex microstructures with lamellar volume fractions of 0.39 for Ti-48-2-2, 0.68 for NCG359E, and a range of 0.5 to 1.0 for GMPX. The cast-to-size ABB-2 samples had a non-uniform microstructure with columnar lamellar colonies at the edge and a more duplex microstructure at the center of the samples. The addition of B in the ABB-23 resulted in a refined lamellar microstructure. Alloy 95A had a thermomechanically treated lamellar microstructure with a fairly large lamellar colony size averaging 288 μm.

The tensile properties of the various alloys are given in Table II. The cast-to-size Ti-48-2-2 had the lowest tensile strength but the highest ductility with an average ultimate tensile strength (UTS) of 422 MPa and a plastic elongation of 1.7% at 25ºC. GMPX had the highest strength with an UTS of 1133 MPa but a slightly lower ductility of 1.3% plastic elongation. After GMPX was exposed to 800 ºC for 200 h, the UTS dropped to 875 MPa at RT and 965 MPa at 650 ºC and the ductility decreased to 0.1% at RT and 0.89% plastic elongation at 650ºC.

The type of impact damage produced depended on the energy level of the projectile. The low energy impacts of 0.22 J or less resulted in shallow dents with very little cracking on the front side of the specimens. At higher energies, front side circumferential cracks, defined here as Hertzian cracks (HZ), initiated at the impact crater and grew toward the specimen edge. These Hertzian cracks extended through the thickness of the specimen, producing an expanding half-cone-shaped crack that resembles the Hertzian cracks commonly observed in other impacted materials. At the highest energies, these cracks often propagated completely through the specimen and resulted in a blow out, i.e., a cone-shaped chunk of material was completely removed. Simultaneous with the frontside cracking, a straight crack was produced on the backside (BS) of the specimen, directly behind the impact. This cracking usually proceeded from the specimen edge to roughly the location opposite the impact crater. The BS cracks form as a result of the tensile stresses resulting from the bending loads caused by the impact. These backside cracks were perpendicular to the loading axis of the fatigue specimen and occasionally branched out in several directions. Examples of Hertzian and backside cracks are shown in Figure 4. For blowouts (BO's), the BS crack length was measured from the edge of the sample to the backside of the Hertzian crack.

The HZ and BS crack lengths are plotted as a function of energy in Fig. 5 for both cast-to-size alloys, Ti-48-2-2 and ABB-2. The TiAl alloy ABB-2 has considerably different chemistry, microstructure, and mechanical properties compared to Ti-48-2-2. Although ABB-2 is significantly stronger than Ti-48-2-2, it has only half the ductility of Ti-48-2-2. The level of

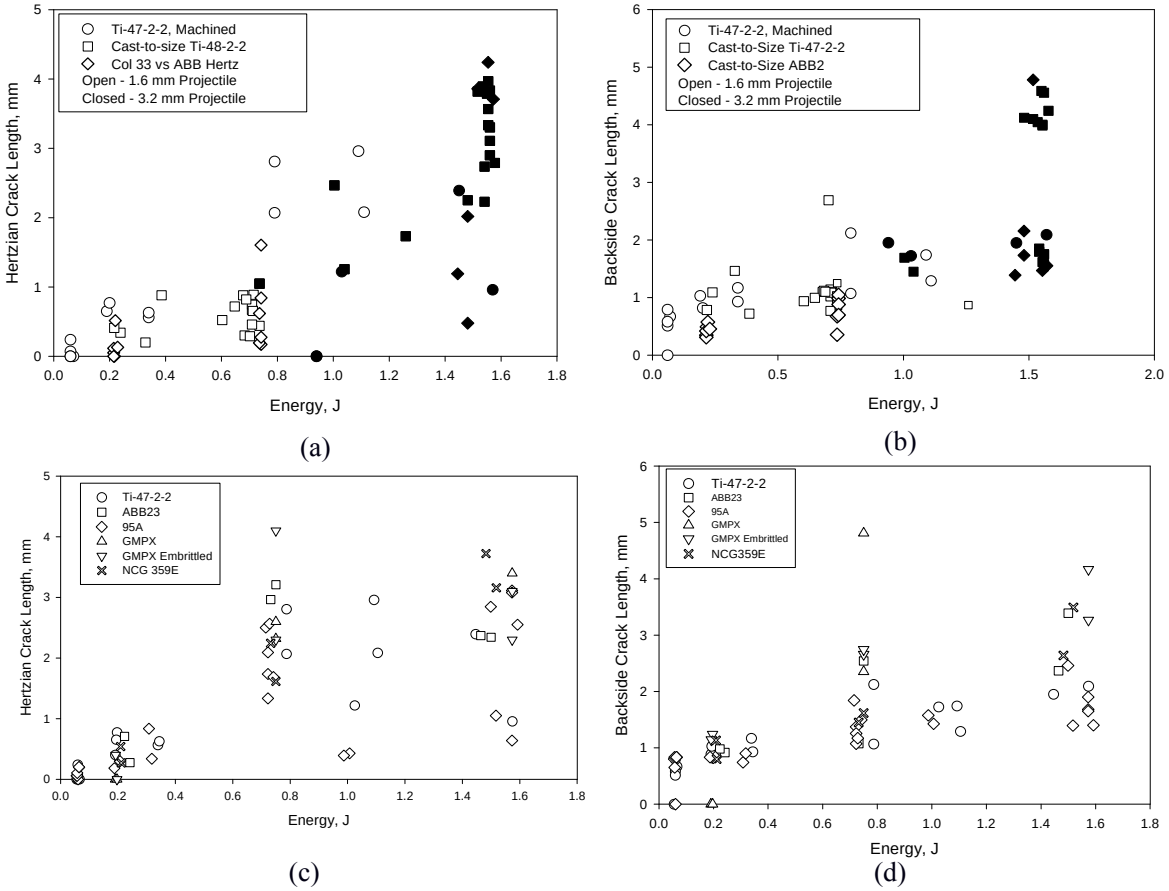

Figure 5. (a) HZ and (b) BS crack length as a function of energy for CTS Ti-48-2-2, machined Ti-47-2-2 and CTS ABB-2. (c) HZ and (d) BS crack length as a function of energy for machined samples from various TiAl alloys.

impact damage was similar for these two alloys at similar impact energies. However, at the lowest impact energy, 0.22 J, half of the impacts on ABB-2 did not produce any apparent HZ or BS cracks, whereas all of the 0.22 J impacts on Ti-48-2-2 resulted in both HZ and BS cracks. The impact sites were metallographially sectioned from several angles to determine the effect of grain orientation on impact damage. Large lamellar grains were fairly common along the specimen surfaces but were not present for all of the ABB-2 samples. The large variability in HZ crack length could be attributed to the presence of these large grains at the specimen surface. The Hertzian cracks appeared to propagate readily when parallel to the lamella orientation, as the crack path is straight and extended in length, Figure 6. Hertzian cracks that run perpendicular to lamellae have a more tortuous and shorter crack path. BS crack length was not influenced by the grain size or orientation. ABB-2 had the same or slightly higher resistance to ballistic impacts compared to Ti-48-2-2 despite ABB-2's lower ductility.

While the cast-to-size specimens offered the best opportunity to match actual blade manufacturing conditions, the cost and difficulty of casting these specimens inhibited progress in studying the impact resistance of additional alloys. Therefore, a machined specimen with a thickness of 2 mm and leading edges resembling those of the cast-to-size specimen was designed. A comparison between crack lengths produced by different impact energies for Ti-48-2-2 cast-to-size samples and Ti-47-2-2 machined samples is given in Figure 5. The type and level of impact damage was comparable at similar impact conditions. The type of impact damage produced depended on both impact energy and the distance from the sample edge to center of impact. Impacts with low energies of 0.06 J resulted in dents but very little cracking on

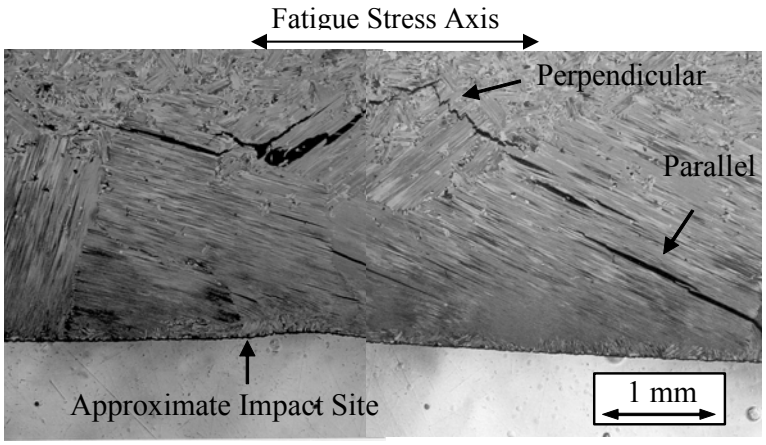

Figure 6. Hertzian cracks propagated easily parallel to large, lamellar grains at the edge of ABB-2 samples but exhibited a more torturous crack path when perpendicular to lamellar grains.

the front side of the specimens for both cast-to-size and machined specimens. At higher E, HZ cracks initiated at the impact crater and grew towards the specimen edge. The 1.6 mm projectiles blew out the machined samples at an E of 0.8 J, significantly lower than the 1.5 J or higher required to blow out the cast-to-size samples. In the range of 0.9 to 1.1 J of energy, the machined Ti-47-2-2 samples were impacted with both 1.6 and 3.2 mm projectiles. The 1.6-mm impacts resulted in blowouts with larger HZ crack lengths. The thinner, machined samples tended to have smaller BS cracks for blowouts in comparison to cast-to-size specimens as the thinner sample shape results in a smaller blown-out piece [5,7]. Despite these slight differences, the cast-to-size and machined samples generally had comparable HZ and BS crack lengths, therefore, a transition was made to the machined sample design for the majority of the alloys.

ABB-23, NCG359E, 95A, and GMPX samples were impacted and characterized giving insight into the effect of processing, microstructure, and tensile properties on ballistic impact resistance. A plot showing the crack lengths as a function of impact energy is shown in Figure 5c,d. GMPX is the highest strength alloy tested and is the only alloy in which cracks did not initiate at the lowest impact energy, 0.2J, on either the front or backside. However, at higher impact energies, the crack lengths of GMPX were similar to all other alloys and therefore the higher tensile strength is of little benefit. Exposing GMPX to 800 ºC for 200 h reduced its resistance to cracking at low energies but had no effect at higher energy impacts.

Crack length due to ballistic impacts have been predicted using finite element models based on ultimate tensile strength (UTS) and ductility by a number of researchers [9, 14-15]. Center impacts are generally easier to model and are well predicted based on a plastic strain criterion [15]. Edge impacts are more complex as bending occurs in both the leading edge plane and a plane normal to it [9, 15]. As seen experimentally [5,7,14,15], the location of the impact, relative to the edge, and impact energy are the most important factors in predicting crack length. It appears that leading edge impacts are best modeled by a combined criterion in which cracking requires both a minimum level of plastic strain and a minimum level of tensile stress. Similar crack lengths have been reported for Ti-48-2-2 and WMS, a higher strength alloy which has similar ductility to Ti-48-2-2 [15]. The explanation given was the ductilities and flow stresses of the two alloys are approximately the same at high strain rates, at least around 1% strain. GMPX has a 23ºC UTS of 1750 MPa at a strain rate of 2100 s^{-1} [16], considerably higher than Ti-48-2-2's UTS of 600 MPa at similar strain rates [17]. While GMPX did resist crack initiation at the lowest impact energies, crack initiation and propagation at higher impact energies was

indistinguishable from any other TiAl alloy. This would not be predicted based on a combined criterion for cracking. Plastic elongations to failure at 1 x 10^{-4} s^{-1} strain rate were in the range of 0.58 to 1.7% at room temperature in the as-received condition for all alloys. Exposed GMPX had a room temperature ductility of only 0.1%, yet exhibited similar crack lengths at high energies to other TiAl alloys. This is not easily explained by existing models.

It was expected that TiAl processing and microstructure would influence the impact behavior of TiAl alloys. Alloys 95A and GMPX are both wrought alloys with 95A being fully lamellar with a large lamellar colony size of 288 μm and GMPX having a refined duplex microstructure, Table I. The impact resistance of the wrought alloys was similar to the other alloys, either cast-to-size or machined from cast plates, and was not influenced by processing. The size of γ grains or lamellar colonies ranged from 4 to 20 μm for GMPX to on the order of 1 mm at the edge of ABB-2 cast-to-size samples. The GMPX had no HZ or BS cracks initiate at 0.2 J of impact energy and ABB-2 had several samples with no HZ or BS cracks at 0.2 J of impact energy. GMPX and ABB-2, the two alloys with the smallest and largest microstructural features, absorbed the largest energy before cracking of all the alloys. Thus, grain or colony size had no effect on impact resistance. ABB-2 had the largest scatter in Hertzian crack length at high impact energies which was related to the large, lamellar grains. The addition of B to ABB-23 reduced the grain size compared to ABB-2 and did decrease the scatter in HZ crack lengths at higher impact energies. However, the overall impact resistance of ABB-23 was similar to ABB-2. The impact resistance of TiAl is remarkably insensitive to processing, microstructure and tensile properties as all alloys had very similar crack lengths at similar impact energies.

Virgin and impacted samples were cycled under high cycle fatigue (HCF) conditions at 650 ºC. The fatigue threshold as a function of impact damage is plotted in Fig. 7 for Ti-48-2-2. A stress at or below this level will not result in any crack growth from the impact cracks and will lead to a run-out condition. Stresses above this level will result in crack growth and rapid failure of the sample. The fatigue strength decreased with increasing impact energy. In general, specimens impacted at low energies failed from backside cracks while at higher energies, the samples failed from HZ cracks. The transition in the failure initiation occurred at approximately 1 J [5,7]. The fracture initiation sites were confirmed by observations of a bluish heat tint on the fracture surfaces after fatigue testing. The color change due to oxidation of impact-initiated cracks was clearly distinguishable from the yellowish color on the surface associated with fatigue crack propagation. The initiation could also be distinguished by the shape of the fracture surfaces. Backside cracks were elliptical in shape and flat fracture surfaces initiated from the backside of the impact. For samples in which fatigue failure initiated from the front side at a Hertzian crack, the fracture surface curved around the impact site, following the HZ crack. At the center of the impact, the fatigue crack proceeded across the width of the specimen. Blowouts failed in a manner similar to the frontside-initiated failure [5,7].

The fatigue strength decreased with increasing crack length, and does so according to a $1/\sqrt{a}$ relationship as described by fracture mechanics, Figs. 7 and 8. A wide variety of alloys with different processing, microstructure, tensile strength and ductility are represented in Fig. 8. A scatter in fatigue strength occurred for the virgin undamaged samples with higher fatigue strength for higher tensile strength alloys. Unexpectedly, the fatigue strength of all impacted samples fit reasonably well on the curve. GMPX has a significantly higher virgin fatigue strength, consistent with its higher tensile strength. However, after cracks form from ballistic impacts, the fatigue strength is undistinguishable from other TiAl alloys. Exposing the GMPX to 800 ºC for 200 h significantly reduces its tensile ductility at room temperature; however, the exposure did not affect the 650 ºC fatigue strength in the as-extruded or impacted condition [3].

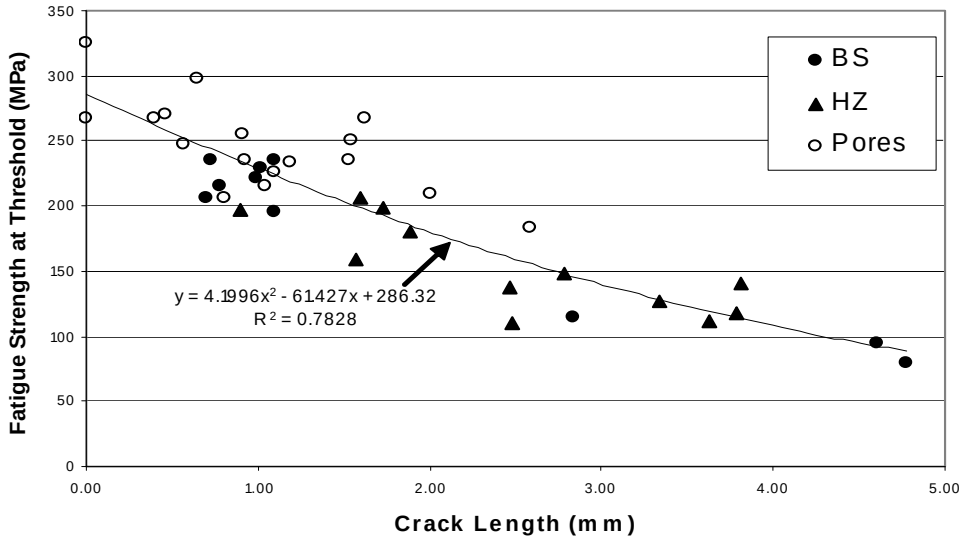

Figure 7. Fatigue strength at threshold as a function of crack length for CTS Ti-48-2-2.

Since the data in Fig. 8 represent various defect geometries, it was not expected that all of the points would fall on one continuous curve. The stress intensity should play a role in the severity of the crack and the threshold approach should give a better representation of the fatigue data. A threshold approach to predicting the fatigue strength has been studied for all of the alloys [8-9] but Figure 8 shows that the threshold approach is not necessary. The geometric factor, F(a/w), is similar for the defect types and sizes studied here. For example, for a crack length of 2 mm and a crack depth of 1 mm, a geometry correction factor for a BS crack is 1.17 and a through Hertzian crack is 1.16. Hence, the defects can be plotted simply as surface crack length. This is fortuitous since surface crack length is the only available information prior to failure on either a sample or an actual component.

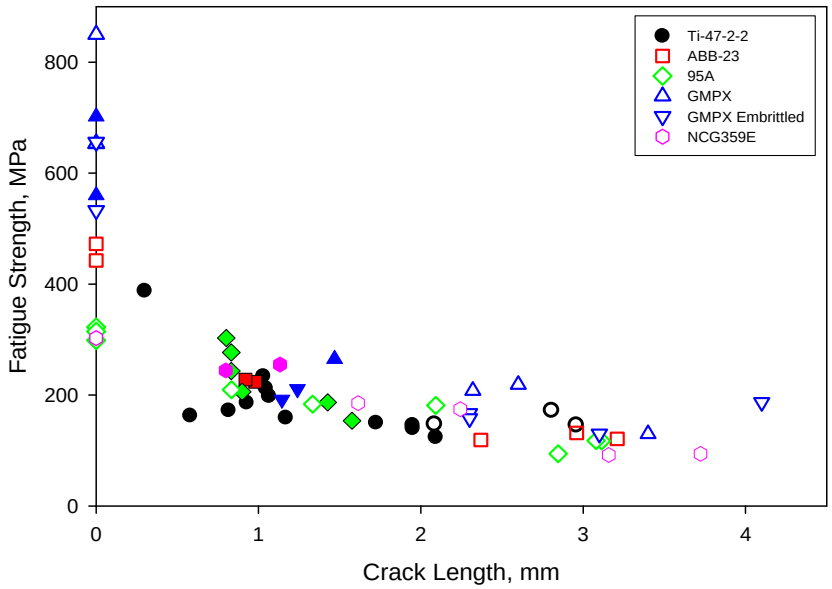

Figure 8. Fatigue strength at threshold for all machined alloys. Open symbols represent virgin and BS initiated failure samples and closed symbols represent samples which failed from HZ initiated cracks.

Summary and Conclusions

Embrittlement due to high temperature exposure is a serious risk to the durability of third generation TiAl alloys. A coating or surface engineering technique which is effective in preventing the ingress of interstitials is critical to the implementation of these alloys. F ion implantation, while it does significantly improve the oxidation resistance of GMPX, does not prevent embrittlement. In fact, the ductility decrease was even more severe for the ion implanted samples.

The ballistic impact resistance of a wide range of TiAl alloys was characterized. The high strength GMPX alloy had slightly improved impact resistance, but this was only observed at fairly low impact energies of 0.2 J. Microstructural features could not be related to impact resistance with the exception that large lamellar grains at the sample edge lead to increased scatter in Hertzian crack length. Backside cracks were not influenced by lamellar content or grain size. Impact samples were cast-to-size or machined from cast plate, forged disk, and extruded bars with no differences in impact properties. The impact resistance of TiAl is remarkably insensitive to processing, microstructure and tensile properties as all alloys had very similar impact resistance. The fatigue strength of all TiAl alloys decreased with increasing crack length according to a $1/\sqrt{a}$ relationship as described by fracture mechanics. A scatter in fatigue strength occurred for virgin samples with higher fatigue strength for higher tensile strength alloys. However, after cracks formed from impacts, the remnant fatigue strength for all TiAl alloys could be predicted based on a single curve and was not related to processing, microstructure, or tensile properties. Consideration of the response of GMPX to both the environmental embrittlement and ballistic impact exposures, calls into question whether the exceptional strength and creep resistance of the third generation alloys can be used in the design of rotating aerospace parts. In fact there is no clear advantage of this alloy over the 1st generation alloy Ti-48-2-2.

Acknowledgements

The authors would like to thank A. Donchev at DECHEMA e.V Karl-Winnacker-Institut for performing the F ion implantation. We would also like to thank C. Austin and T. Kelly from GEAE, M.Y. Nazmy and M. Staubli from Alstom Power, D. Clemens from Howmet Research Corp., and Y.W. Kim from UES, Inc. for materials and helpful discussions.

References

1. C.M. Austin and T.J. Kelly, in Superalloys 1996, ed. by R.D. Kissenger, D.J. Deye, D.L. Anton, A.D. Cetel, M.V. Nathal, T.M. Pollock, and D.A. Woodford, TMS, Warrandale, PA, 1996, p.539.

2. F. Appel et al., "Design, Properties and Processing of Novel TiAl Alloys," *Structural Intermetallics 2001*, eds. K.J Hemker et al., (Warrendale, PA: TMS, 2001), 63-72.

3. S.L. Draper et al., "Effect of exposure on the mechanical properties of Gamma MET PX," *Intermetallics*, 13 (2005) 1014-1019.

4. A. Donchev et al., "Improvement of the oxidation behaviour of TiAl-alloys by treatment with halogens," *Intermetallics,* 14 (2006) 1168-1174.

5. S.L. Draper et al., "The effect of ballistic impacts on the high-cycle fatigue properties of Ti-48Al-2Nb-2Cr," Metall. Trans., 32A (2001) 2743-58.

6. J.M Larsen et al., *Gama Titanium Aluminides,* eds. Y.W. Kim, R. Wagner and M. Yamaguchi, (Warrendale, PA: TMS, 1995), 821-834.

7. S.L. Draper et al., *Structural Intermetallics 2001*, eds. K.J Hemker et al., (Warrendale, PA: TMS, 2001), 295-304.

8. B.A. Lerch et al., *Gamma Titanium Aluminides 2003*, eds. Y-W. Kim, H. Clemens and A.H. Rosenberger (Warrendale, PA: TMS, 2003), 477-483.

9. S.L. Draper et al., "Durability Assessment of Gamma TiAl – Final Report," NASA TM – 2004-212303, NASA - Glenn Research Center, Cleveland, OH (2004).

10. J.A. Collins, *Failure of Materials in Mechanical Design,* (New York, NY: John Wiley & Sons, 1993), 379-381.

11. S.K. Planck, A. H. Rosenberger, Mater. Sci. Eng., A325 (2002), 270-280.

12. T.J. Kelly et al., Scripta Metal. Mater., 30 (1994), 1105-10.

13. D.S. Lee, M.A. Stucke, and D.M. Dimiduk, Mater Sci. Eng. A (1995), 192-3.

14. R. Smith et al., *Structural Intermetallics 2001*, eds. K.J Hemker et al., (Warrendale, PA: TMS, 2001), 259-268.

15. V.T. McKenna et al., "Cracking in γ-TiAl due to High Speed Particle Impact", Metall. Trans., 33A, 2002, 581-589.

16. M. Shazly, V. Prakash, and S. Draper, "Mechanical Behavior of Gamma-Met PX under Uniaxial Loading at Elevated Temperatures and High Strain Rates," Int. J. Solids Struct., 41 (2004), 6485-6503.

17. S.A. Maloy and G.T. Gray III, "High Strain Rate Deformation of Ti-48Al-2Nb-2Cr," Acta Mater., 44, No. 5, 1741-56.